Biosensors and Bioelectronics 36 (2012) 262–266

Contents lists available at SciVerse ScienceDirect

Biosensors and Bioelectronics

journal homepage: www.elsevier.com/locate/bios

Short communication

# Novel snowflake-like Pt–Pd bimetallic clusters on screen-printed gold nanofilm electrode for $H_2O_2$ and glucose sensing

Xiangheng Niu [a], Chen Chen [a], Hongli Zhao [a,*], Yan Chai [a], Minbo Lan [a,b,*]

[a] Shanghai Key Laboratory of Functional Materials Chemistry, and Research Centre of Analysis and Test, East China University of Science and Technology, Shanghai 200237, PR China

[b] State Key Laboratory of Bioreactor Engineering, East China University of Science and Technology, Shanghai 200237, PR China

ARTICLE INFO

*Article history:*
Received 4 February 2012
Received in revised form
14 March 2012
Accepted 14 March 2012
Available online 7 April 2012

*Keywords:*
Snowflake-like Pt–Pd nanoclusters
$H_2O_2$
Glucose oxidase
Glucose

ABSTRACT

Novel snowflake-like Pt–Pd bimetallic nanoclusters (Pt–PdBNC) were synthesized on a screen-printed gold nanofilm electrode (SPGFE) substrate by electrochemically reducing precursors with a new constant potential/multi-potential step deposition strategy. The electrocatalytic behavior of the modified electrode (SPGFE/Pt–PdBNC) towards $H_2O_2$ was investigated. The results indicate that the as-prepared Pt–PdBNC significantly enhances the electrochemical reduction of $H_2O_2$ in neutral media, exhibiting preferable electrocatalytic performance compared to Pt and Pd monometallic nanoclusters. Under optimum conditions, SPGFE/Pt–PdBNC offers linear responses for $H_2O_2$ in the concentration range from 0.005 to 6 mM with an ultrahigh sensitivity of 804 mA $M^{-1}$ $cm^{-2}$ and excellent selectivity. Furthermore, glucose oxidase was immobilized on the Pt–PdBNC structure, and the fabricated biosensor presents favorable properties for glucose sensing.



## 1. Introduction

Nowadays there is still a great demand for developing glucose biosensors due to their applications in blood sugar monitoring (Berhan et al., 2011). Many approaches have been explored for glucose sensing in the past decades, and the glucose oxidase method is generally considered as an efficient route to detect glucose because of its high sensitivity and preeminent selectivity. In addition, $H_2O_2$ sensing, which can be used to determine the blood glucose content, is also of great importance and attracts considerable attention (Chen et al., 2011).

Intense efforts have been paid on nanostructured materials due to their distinctive properties (Willner and Willner, 2010). As an outstanding electrode material, nanostructured Pt is of particular interest for applications in catalysis and sensing owing to its favorable electrochemical stability and prominent catalytic activity (Chen and Holt-Hindle, 2010). Similarly, Pd is well known as a conventional metallic catalyst, and has gained widespread applications in the fields of organic synthesis (Wu et al., 2011), direct fuel cell (Bianchini and Shen, 2009), etc. Compared to monometallic catalysts, multi-metallic composites are more promising candidates for practical applications because the latter exhibit preferable catalytic properties with synergistic effects (Becerik et al., 1999; Xu et al., 2011). Among these composites, Pt–Pd alloys have drawn much interest. Lim et al. (2009) find that Pt–Pd composites enhance the electrocatalytic reduction response of oxygen. Wang et al. (2011) also demonstrate that Pt–Pd alloy nanoparticles provide better catalytic performance for $H_2O_2$ reduction and nitrite oxidation. These encouraging results attract growing attention on the study of multi-metallic catalysts.

In recent years, three-dimensional (3D) nanostructures have specially obtained much attention because of their beneficial skeletons (Zhao et al., 2007; Thompson and Brook, 2008). Generally, 3D structures can expose abundant active sites. Besides, electroconductive 3D framework offers sufficient electron transfer pathways. Xiao et al. (2011) propose a 3D Pt nanoflower-modified electrode to electrocatalyze glucose, and find that the decorated electrode offers a high sensitivity for glucose sensing. It is believed that 3D multi-metallic nanostructures, integrating advantages of the 3D structure with beneficial synergistic effects of alloy catalysts, can also provide attractive catalytic qualities. There are, however, few reports involving the intensive investigation of 3D multi-metallic catalysts.

Here we propose a new electrodeposition strategy to synthesize snowflake-like Pt–Pd bimetallic nanoclusters (Pt–PdBNC) on a screen-printed gold nanofilm electrode (SPGFE) substrate. The 3D Pt–PdBNC structure was obtained by electrochemically reducing precursors with a constant potential at first and later multi-potential step deposition. The electrocatalytic behavior of the fabricated SPGFE/Pt–PdBNC towards $H_2O_2$ was discussed. Furthermore, glucose oxidase (GOx) was immobilized on the proposed structure to prepare glucose biosensors.

* Corresponding authors. Tel.: +86 21 64253574; fax: +86 21 64252947.
*E-mail addresses:* honglizhao@ecust.edu.cn (H. Zhao), minbolan@ecust.edu.cn (M. Lan).

0956-5663/$ - see front matter © 2012 Elsevier B.V. All rights reserved.
http://dx.doi.org/10.1016/j.bios.2012.03.030

## 2. Experimental

### 2.1. Chemicals and apparatus

$H_2PtCl_6 \cdot 6H_2O$ (Aladdin Chemistry Co.) and $PdCl_2$ (Sinopharm Chemical Reagent Co.) were commercially obtained. $H_2O_2$ (Sinopharm Chemical Reagent Co.) was stored at 4 °C and diluted to required concentrations before use. GOx (from *Aspergillus niger*, EC 1.1.3.4, type VII, 192,000 unit/g, Sigma-Aldrich Co.) solution was also prepared before use. β-D(+)-glucose (Sigma-Aldrich Co.) solution was left overnight to allow equilibration of anomers. 0.1 M phosphate buffer solution (PBS, pH=6.9) was employed as the supporting electrolyte.

Scanning electron microscopy (SEM, JSM-6360LV) was used to observe the morphology of nanostructures, and energy dispersive X-ray spectrometer (EDS, Falcon) was used to determine the elemental component. All electrochemical experiments were carried out on a CHI 440 A electrochemical station (CHI Instruments Inc.) at room temperature (25 ± 2 °C). A conventional three-electrode configuration consisting of a screen-printed working electrode, a Pt wire counter electrode and a saturated Ag/AgCl reference electrode was employed.

### 2.2. Preparation of SPGFE/Pt–PdBNC

The preparation of SPGFE has been described in previous work (Teng et al., 2009; Niu et al., 2011), and the thickness of the gold film is 75 ± 5 nm. Firstly, a SPGFE was immersed into a mixture of 1 mM $H_2PtCl_6$ and 1 mM $PdCl_2$ for 5 min to make the precursor solution wet the substrate; then a constant potential (CP) of −0.4 V was applied to reduce Pt(IV) and Pd(II) for 20 s; afterwards, a multi-potential step (MPS) deposition from +0.5 V (0.2 s) to −0.4 V (10 s) for 50 cycles was carried out; finally, the electrode was carefully rinsed with adequate water and dried. For comparison, Pt monometallic nanoclusters (PtMNCs) and Pd monometallic nanoclusters (PtMNCs) were also prepared with similar processes, and 2 mM $H_2PtCl_6$ and 2 mM $PdCl_2$ precursor solutions were used in the deposition section, respectively. Furthermore, preparations of Pt–Pd nanostructures with only either CP (−0.4 V for 530 s) or MPS (from +0.5 V (0.2 s) to −0.4 V (10 s) for 50 cycles) deposition were carried out.

### 2.3. Fabrication of glucose biosensor

A cross-linking method with glutaraldehyde and bovine serum albumin (BSA) was adopted to immobilize GOx on the as-prepared SPGFE/Pt–PdBNC. 500 μL GOx (5 mg/mL) was well mixed with 100 μL BSA (10 mg/mL) and 100 μL glutaraldehyde (2 wt%); then 10 μL of the mixture solution was dropped on the SPGFE/Pt–PdBNC working area and allowed to dry overnight at 4 °C; afterwards, the GOx-modified electrode was carefully rinsed with 0.1 M PBS to get rid of the poorly adsorbed GOx. The obtained SPGFE/Pt–PdBNC/GOx was stored in a 0.1 M PBS (pH=6.9) solution at 4 °C when not in use.

### 2.4. Electrochemical measurements

All electrochemical experiments were accomplished on the aforementioned station. The electrocatalytic properties of different electrodes for $H_2O_2$ were evaluated with cyclic voltammetry and chronoamperometry. All amperometric measurements were implemented by successive addition of analytes into 0.1 M PBS (pH=6.9) with a constant stir.

## 3. Results and discussion

### 3.1. Characterization of SPGFE/Pt–PdBNC

The SEM image (Fig. 1(A)) reveals that the as-prepared Pt–Pd composites are well dispersed on the substrate surface, and the higher resolution image indicates that a snowflake-like cluster structure with a diameter of approximately 800 nm is obtained. The formation of this 3D Pt–Pd nanostructure can be explained by the heterogeneous seeded growth mechanism (Lim and Xia, 2011). In the Pt(IV)/Pd(II) bath, the initial constant potential of −0.4 V for 20 s induces the formation of numerous crystal seeds, then the following multi-potential step electrodeposition promotes the growth of colloidal nanostructures on the previously formed seeds. Owing to the close lattice match between these two metals (Pt and Pd have a lattice mismatch of only 0.77%), the seeded growth is easily undergone (Lim et al., 2009; Peng and Yang, 2009), finally producing 3D snowflake-like Pt–Pd nanoclusters. This capacious and poriferous structure provides large surface areas and abundant active sites, and is beneficial for heterogeneous catalysis. The EDS pattern (Fig. 1(B)) displays the typical diffractions of Pt and Pd, revealing the successful preparation of Pt–Pd composites using the electrodeposition method. Fig. 1(C) presents cyclic voltammograms of different electrodes in 0.5 M $H_2SO_4$ solutions. The bare SPGFE offers a specific peak of Au at +0.8 V. At SPGFE/PtMNC and SPGFE/PdMNC, the Au peak is seriously reduced. Both the two electrodes provide a remarkable peak at around +0.3 V, assigned to Pt and Pd oxides (Qu et al., 2007). The proposed SPGFE/Pt–PdBNC also offers a similar expanded peak of the Pt–Pd composite. Besides, cyclic voltammograms in the common ferricyanide system (Fig. 1(D)) reveal that SPGFE/Pt–PdBNC exhibits enhanced performance for promoting electron transfer than other electrodes.

### 3.2. Electrocatalytic detection of $H_2O_2$

Fig. 2(A) depicts cyclic voltammograms of different electrodes in 0.1 M PBS containing 10 mM $H_2O_2$. The bare SPGFE presents no notable response upon $H_2O_2$ in the selected potential window, revealing that the substrate hardly exhibits electrocatalytic capability for $H_2O_2$. When PtMNC and PdMNC are introduced, both nanostructures provide a remarkable reduction signal of $H_2O_2$ at approximately −0.1 V, indicating that both PtMNC and PdMNC can greatly electrocatalyze the reduction of $H_2O_2$ in neutral media, attributing to the attractive catalytic activities of Pt and Pd. Furthermore, a detectable but poor oxidation response of $H_2O_2$ is observed at potentials more positive than +0.4 V. Compared to PtMNC and PdMNC, the Pt–PdBNC structure, which provides a higher current response at a little more positive potential, exhibits preferable catalytic performance for $H_2O_2$ reduction. This enhanced performance mainly results from synergistic effects of Pt–Pd alloys. On the one hand, bimetallic nanostructure may offer more catalytic sites for $H_2O_2$ reduction compared to monometallic catalysts (Li et al., 2004; Wang et al., 2009); on the other hand, the electrocatalytic activity of each metal in alloys perhaps gets some enhancement (Wang et al., 1996).

Fig. 2(B) shows chronoamperometric responses of different electrodes upon successive addition of $H_2O_2$ at −0.4 V. SPGFE/PtMNC, SPGFE/PdMNC and SPGFE/Pt–PdBNC display distinct current increases stepwise upon $H_2O_2$ concentrations, and the latter provides the most sensitive responses for $H_2O_2$ reduction. These amperometric results also demonstrate enhancement of the overall electrocatalytic qualities of bimetallic structures in contrast to monometallic catalysts. A comparison of Pt–Pd nanostructures prepared with different deposition methods was further made by

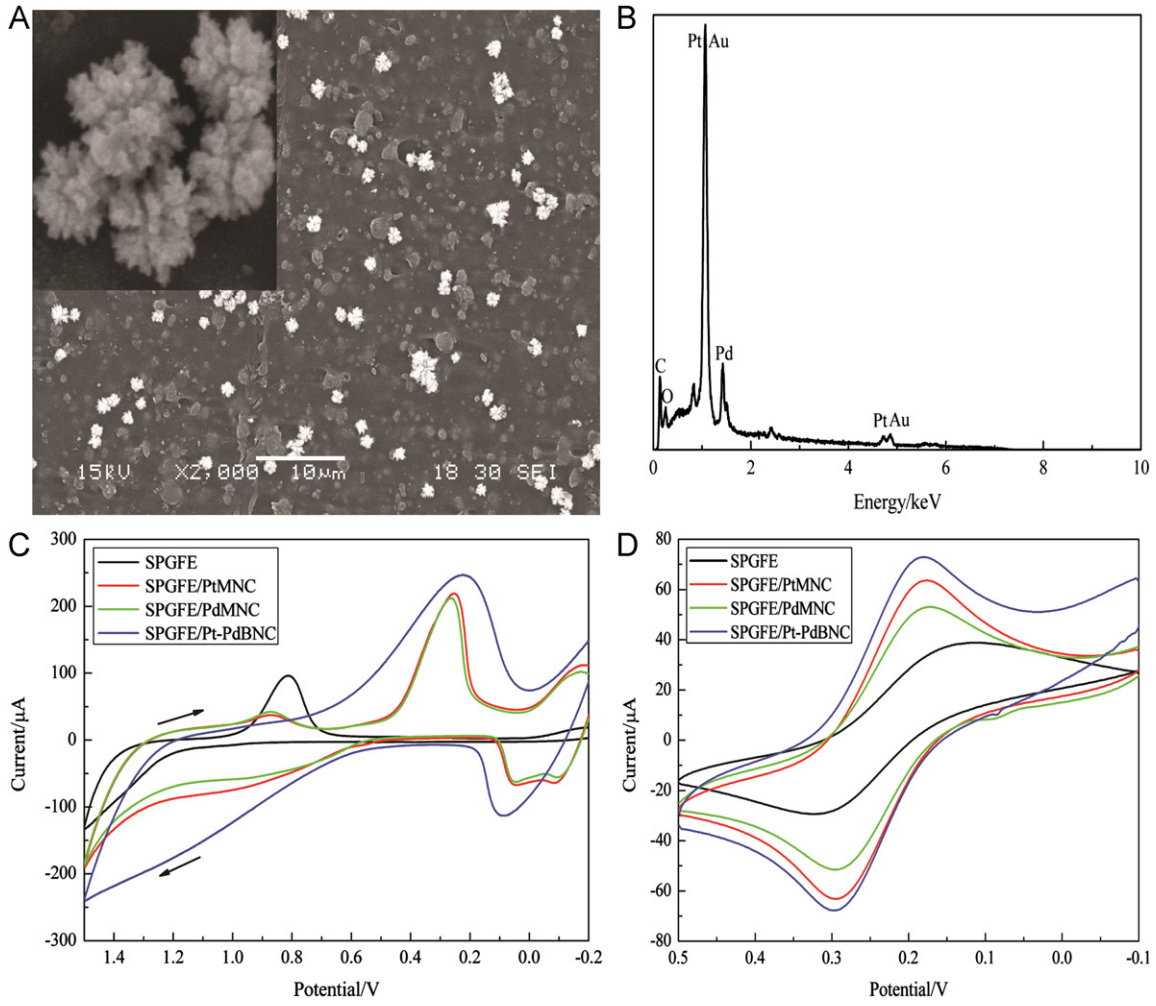


**Fig. 1.** (A) SEM image of the as-synthesized Pt–PdBNC; (B) EDS pattern of Pt–PdBNC/SPGFE; (C) Cyclic voltammograms of different electrodes in 0.5 M $H_2SO_4$ at a scan rate of 100 mV/s; (D) Cyclic voltammograms of different electrodes in 2 mM $K_3[Fe(CN)_6]$ containing 0.5 M KCl at a scan rate of 100 mV/s.

testing their electrocatalytic performance for $H_2O_2$ reduction. The SEM image (Fig. S1(A), Supporting Information) indicates that Pt–Pd composites prepared with the CP deposition exhibit serious agglomeration, dramatically reducing surface active sites. As a result, the modified electrode shows the least sensitive responses upon $H_2O_2$ (Fig. S1(C)). While the MPS and integrated CP/MPS deposition form relatively dispersed clusters (Fig. S1(B)). Among these structures, Pt–Pd nanoclusters prepared with the integrated CP/MPS electrodeposition exhibit the most sensitive responses for $H_2O_2$ reduction.

With the optimum precursor composition (Fig. S2(A)) and applied potential (Fig. S2(B)), the overall electroanalytical performance of the fabricated SPGFE/Pt–PdBNC for $H_2O_2$ was evaluated. Fig. 3(A) depicts amperometric responses of SPGFE/Pt–PdBNC upon successive addition of $H_2O_2$ in 0.1 M PBS, and the inset presents the amplified current details upon low concentrations of $H_2O_2$. The fabricated electrode shows very fast response achieving 95% of the steady-state current within 2 s. The current responses linearly increase with $H_2O_2$ concentrations from 0.005 to 6 mM with a correlation coefficient of 0.9962 (Fig. 3(B)). The limit of detection (LOD) is calculated to be 0.87 μM based on the signal/noise protocol (S/N=3). Moreover, a sensitivity of 804 mA $M^{-1}$ $cm^{-2}$ is obtained. Compared to nonenzymatic electrochemical sensors fabricated on other nanostructures (Table S1, Supporting Information), the proposed Pt–PdBNC provides comparable or even better linear range and LOD. More importantly, Pt–PdBNC offers an ultrahigh sensitivity for $H_2O_2$ detection. Such excellent sensitivity is attributed to the outstanding electrocatalytic activity of nanostructured Pt and Pd and their beneficial synergistic effects. Furthermore, eight amperometric measurements of 0.5 mM $H_2O_2$ at a single electrode result in repeatable data with a relative standard deviation (RSD) of 4.2%. Besides, eight duplicate electrodes are used to evaluate the reliability, and a RSD of 7.1% is obtained for 0.5 mM $H_2O_2$ sensing. As shown in Fig. S3, no notable influence from addition of 0.5 mM ascorbic acid (AA), dopamine (DA), uric acid (UA) and glucose on measurements of 0.5 mM $H_2O_2$ is observed, indicating that the fabricated electrode can selectively detect $H_2O_2$ in the presence of these common species. The modified electrode is also demonstrated capable of detecting $H_2O_2$ in spiked samples reliably.

### 3.3. Glucose biosensor based on SPGFE/Pt–PdBNC

GOx was further immobilized on SPGFE/Pt–PdBNC to fabricate a glucose biosensor. Fig. S4 depicts amperometric responses of the fabricated SPGFE/Pt–PdBNC/GOx for successive addition of glucose in 0.1 M PBS. The responses increase stepwise with the increasing concentrations of glucose. The fabricated biosensor provides linear currents for glucose in the concentration range of 0–16 mM with a correlation coefficient of 0.9981. The LOD is further calculated to be 10 μM. Compared to enzyme-free or GOx-based amperometric sensors fabricated on other nanostructures (Table S2, Supporting Information), the proposed biosensor

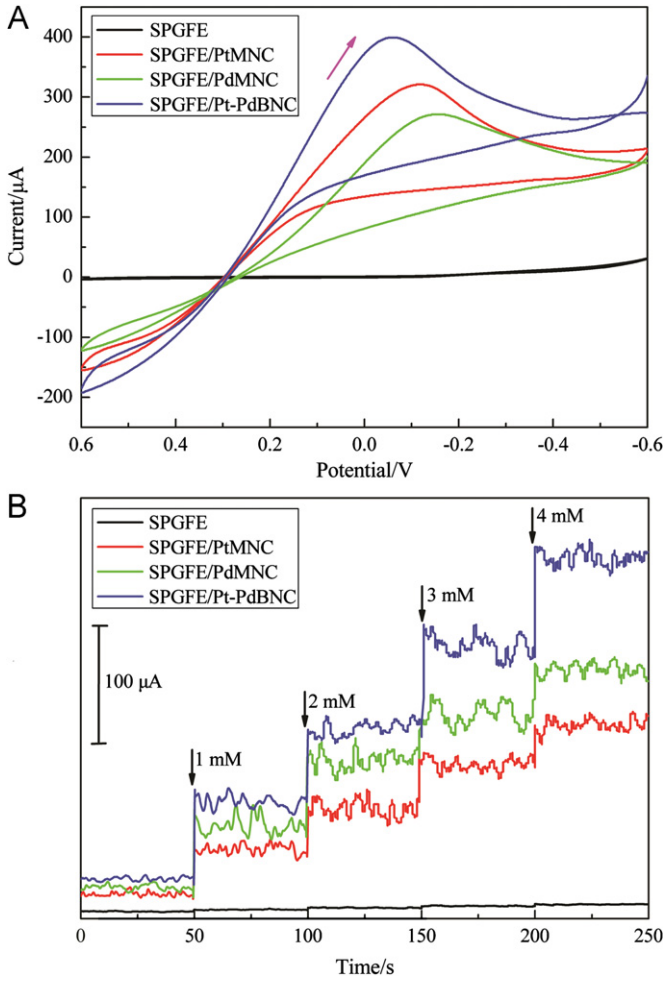


**Fig. 2.** (A) Cyclic voltammograms of different electrodes in 0.1 M PBS containing 10 mM $H_2O_2$ at a scan rate of 100 mV/s; (B) Amperometric responses of different electrodes upon successive addition of 0–4 mM $H_2O_2$ in 0.1 M PBS at −0.4 V with a constant stir.

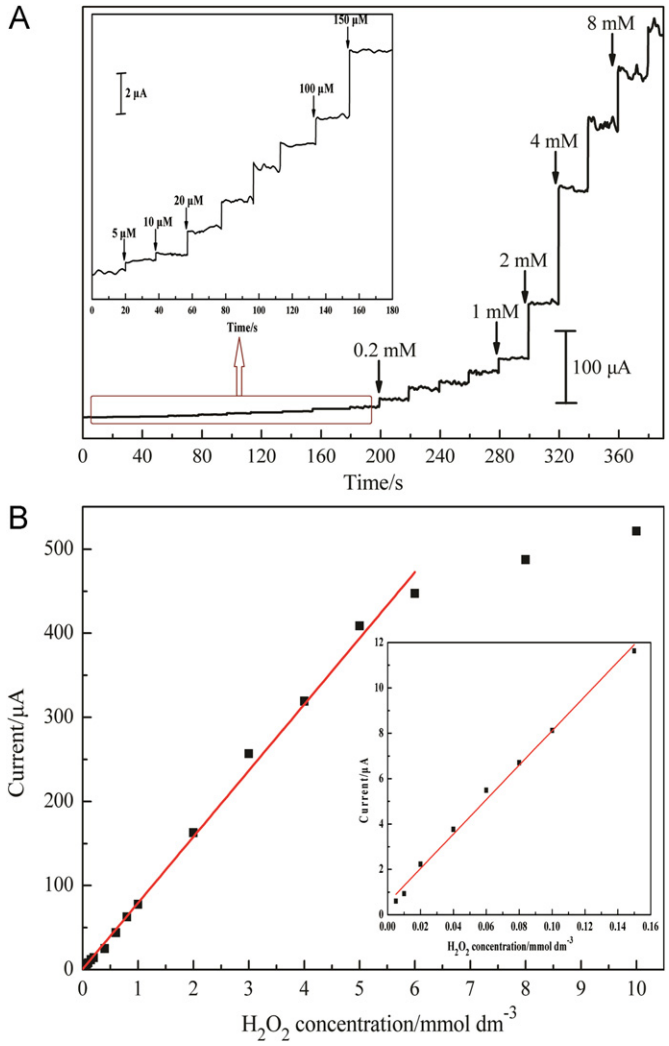


**Fig. 3.** (A) Amperometric responses of SPGFE/Pt–PdBNC upon successive addition of $H_2O_2$ in 0.1 M PBS at −0.4 V with a constant stir; (B) Calibration curve for the amperometric responses upon $H_2O_2$ concentrations.

presents wider linear range and satisfactory LOD, ascribing to the preeminent sensitivity of SPGFE/Pt–PdBNC for $H_2O_2$ sensing. Measurements of 5 mM glucose at six duplicate biosensors are carried out, and a RSD of 5.1% demonstrates a good repeatability of these biosensors. The selectivity test (Fig. S5) reveals that 0.5 mM D(+)-galactose, D-fructose, D(+)-xylose, D-ridose and AA provide no interference for glucose sensing. However, it is comprehensible that the addition of $H_2O_2$ offers a great increase of current. Simulative blood samples prepared with a 0.1 M PBS solution (pH=7.4) containing 6 mM glucose, 0.1 mM AA, 0.1 mM 4-acetamidophenol (AP), 0.1 mM DA, 0.02 mM UA and 0.15 mM chloride ions (Wang et al., 2008) are tested, and a result of $6.13 \pm 0.17$ mM ($n=3$) reveals that the fabricated biosensor has great potential applications for real sample measurements.

## 4. Conclusion

We demonstrate the facile preparation of 3D snowflake-like Pt–PdBNC by electrochemically reducing precursors. The synthesized Pt–PdBNC provides enhanced electrocatalytic performance for $H_2O_2$ reduction in neutral media than PtMNC and PdMNC. The as-prepared SPGFE/Pt–PdBNC exhibits wide linear range, ultrahigh sensitivity and excellent selectivity for detecting $H_2O_2$. The fabricated SPGFE/Pt–PdBNC/GOx biosensor also presents favorable properties for glucose sensing.

## Acknowledgments

This work was financially supported by Science and Technology Commission of Shanghai Municipality (STCSM, contract no. 10dz2220500 and 10391901600) and Ministry of Education of the People's Republic of China (contract no. WK1014051).

## Appendix A. Supporting information

Supplementary data associated with this article can be found in the online version at http://dx.doi.org/10.1016/j.bios.2012.03.030.

## References

Becerik, I., Suzer, S., Kadırgan, F., 1999. Journal of Electroanalytical Chemistry 476, 171–176.
Berhan, Y., Waernbaum, I., Lind, T., Möllsten, A., Dahlquist, G., 2011. Diabetes 60, 577–581.
Bianchini, C., Shen, P.K., 2009. Chemical Reviews 109, 4183–4206.
Chen, A.C., Holt-Hindle, P., 2010. Chemical Reviews 110, 3767–3804.
Chen, W., Cai, S., Ren, Q.Q., Wen, W., Zhao, Y.D., 2011. Analyst http://dx.doi.org/10.1039/c1an15738h.
Li, H.Q., Xin, Q., Li, W.Z., Zhou, Z.H., Jiang, L.H., Yang, S.H., Sun, G.Q., 2004. Chemical Communications 23, 2776–2777.

Lim, B., Jiang, M.J., Camargo, P.H.C., Cho, E.C., Tao, J., Lu, X.M., Zhu, Y.M., Xia, Y.N., 2009. Science (New York, NY) 324, 1302–1305.
Lim, B., Xia, Y.N., 2011. Angewandte Chemie-International Edition 50, 76–85.
Niu, X.H., Ding, Y.L., Chen, C., Zhao, H.L., Lan, M.B., 2011. Sensors and Actuators, B: Chemical 158, 383–387.
Peng, Z.M., Yang, H., 2009. Journal of the American Chemical Society 131, 7542–7543.
Qu, F.L., Yang, M.H., Shen, G.L., Yu, R.Q., 2007. Biosensors and Bioelectronics 22, 1749–1755.
Teng, Y.J., Zuo, S.H., Lan, M.B., 2009. Biosensors and Bioelectronics 24, 1353–1357.
Thompson, D.B., Brook, M.A., 2008. Journal of the American Chemical Society 130, 32–33.
Wang, H., Bo, X.J., Bai, J., Wang, L.X., Guo, L.P., 2011. Journal of Electroanalytical Chemistry 662, 281–287.
Wang, J., Pamidi, P.V.A., Cepria, G., 1996. Analytica Chimica Acta 330, 151–158.
Wang, J.P., Thomas, D.F., Cheng, A.C., 2008. Analytical Chemistry 80, 997–1004.
Wang, W.M., Huang, Q.H., Liu, J.Y., Zou, Z.Q., Zhao, M.Y., Vogel, W., Yang, H., 2009. Journal of Catalysis 266, 156–163.
Willner, I., Willner, B., 2010. Nano Letters 10, 3805–3815.
Wu, X.F., Neumann, H., Beller, M., 2011. Chemical Society Reviews 40, 4986–5009.
Xiao, X.Y., Montano, G.A., Edwards, T.L., Washburn, C.M., Brozik, S.M., Wheeler, D.R., Burckel, D.B., Polsky, R., 2011. Biosensors and Bioelectronics 26, 3641–3646.
Xu, J.G., Wilson, A.R., Rathmell, A.R., Howe, J., Chi, M.F., Wiley, B.J., 2011. ACS Nano 5, 6119–6127.
Zhao, Y., Fan, L.Z., Zhong, H.Z., Li, Y.F., Yang, S.H., 2007. Advanced Functional Materials 17, 1537–1541.